ISSN 1674-1056
http://cpb.iphy.ac.cn
http://iopscience.iop.org/cpb
中国物理 B
Chinese Physics
中国物理 Chinese Physics B

Room-temperature strong coupling between dipolar plasmon resonance in single gold nanorod and two-dimensional excitons in monolayer WSe_2

Jinxiu Wen(温锦秀)[1,4], Hao Wang(汪浩)[1,3], Huanjun Chen(陈焕君)[1,2], Shaozhi Deng(邓少芝)[1,2], Ningsheng Xu(许宁生)[1,2]

Citation: Chin. Phys. B . 2018, 27(9): 096101. **doi:** 10.1088/1674-1056/27/9/096101

Journal homepage: http://cpb.iphy.ac.cn; http://iopscience.iop.org/cpb

What follows is a list of articles you may be interested in

Light trapping and optical absorption enhancement in vertical semiconductor Si/SiO_2 nanowire arrays

Ying Wang(王莹), Xin-Hua Li(李新化)

Chin. Phys. B . 2018, 27(2): 026102. **doi:** 10.1088/1674-1056/27/2/026102

Synthesis and magnetotransport properties of Bi_2Se_3 nanowires

Kang Zhang(张亢), Haiyang Pan(潘海洋), Zhongxia Wei(魏仲夏), Minhao Zhang(张敏昊), Fengqi Song(宋凤麒), Xuefeng Wang(王学锋), Rong Zhang(张荣)

Chin. Phys. B . 2017, 26(9): 096101. **doi:** 10.1088/1674-1056/26/9/096101

Local microstructural analysis for $Y_2O_3/Eu^{3+}/Mg^{2+}$ nanorods by Raman and photoluminescence spectra under high pressure

Jin-Hua Wang(王金华), Ze-Peng Li(李泽朋), Bo Liu(刘波), Bing-Bing Liu(刘冰冰)

Chin. Phys. B . 2017, 26(2): 026101. **doi:** 10.1088/1674-1056/26/2/026101

Studies on the nucleation of MBE grown III-nitride nanowires on Si

Yanxiong E(鄂炎雄), Zhibiao Hao(郝智彪), Jiadong Yu(余佳东), Chao Wu(吴超), Lai Wang(汪莱), Bing Xiong(熊兵), Jian Wang(王健), Yanjun Han(韩彦军), Changzheng Sun(孙长征), Yi Luo(罗毅)

Chin. Phys. B . 2017, 26(1): 016103. **doi:** 10.1088/1674-1056/26/1/016103

Magnetostatic interaction in electrodeposited Ni/Au multilayer nanowire arrays

Li-Zhong He(何丽忠), Li-Rong Qin(秦丽溶), Jian-Wei Zhao(赵建伟), Ying-Ying Yin(殷营营), Yu Yang(杨瑜), Guo-Qing Li(李国庆)

Chin. Phys. B . 2016, 25(8): 086101. **doi:** 10.1088/1674-1056/25/8/086101

SPECIAL TOPIC — Nanophotonics

Room-temperature strong coupling between dipolar plasmon resonance in single gold nanorod and two-dimensional excitons in monolayer WSe_2*

Jinxiu Wen(温锦秀)[1,4], Hao Wang(汪浩)[1,3], Huanjun Chen(陈焕君)[1,2,†], Shaozhi Deng(邓少芝)[1,2,‡], and Ningsheng Xu(许宁生)[1,2]

[1] State Key Laboratory of Optoelectronic Materials and Technologies, Guangdong Province Key Laboratory of Display Material and Technology, Sun Yat-sen University, Guangzhou 510275, China

[2] School of Electronics and Information Technology, Sun Yat-sen University, Guangzhou 510006, China

[3] School of Physics, Sun Yat-sen University, Guangzhou 510275, China

[4] School of Applied Physics and Materials, Wuyi University, Jiangmen 529020, China

(Received 16 April 2018; revised manuscript received 23 May 2018; published online 10 August 2018)

All-solid-state strong coupling systems with large vacuum Rabi splitting energy have great potential applications in future quantum information technologies, such as quantum manipulations, quantum information storage and processing, and ultrafast optical switches. Monolayer transition metal dichalcogenides (TMDs) have recently been explored as excellent candidates for the observation of solid-state strong coupling phenomena. In this work, from both experimental and theoretical aspects, we explored the strong coupling effect by integrating an individual plasmonic gold nanorod into the monolayer tungsten diselenide (WSe_2). Evident anti-crossing behavior was observed from the coupled energy diagram at room temperature; a Rabi splitting energy of 98 meV was extracted.

Keywords: Au nanorod-WSe_2 heterostructures, strong coupling, all-solid-state system, room temperature

PACS: 61.46.Km, 73.20.Mf, 71.45.Gm, 61.46.Hk **DOI:** 10.1088/1674-1056/27/9/096101

1. Introduction

By integrating a specific quantum emitter into an optical cavity, its optical response can be modified substantially owing to the variation in the local electromagnetic environment within the cavity. In particular, if the interaction between the emitter and optical cavity is sufficiently strong to overwhelm their respective dissipation rates, a strong coupling regime is achieved.[1,2] In this regime, hybridized energy states with part-light and part-matter characteristics are formed, which can be observed from the optical spectra of the system as mode splitting, or, in a quantum mechanics language, the Rabi splitting (RS). The strong coupling effects can form the basis of many quantum optics applications, such as quantum manipulation, quantum information storage and processing, and ultrafast single-photon switches.[3–5] Consequently, several systems with a strong coupling effect have been proposed and systematically studied, including atoms placed in optical microcavities,[6] quantum dots integrated with photonic crystals,[2,7] quantum wells embedded into distributed Bragg reflectors (DBR) cavities,[8] and organic molecules coupled with plasmonic nanocavities.[9–11]

From an application point of view, an all-solid-state system operating at room temperature and having easily accessible large RS is preferred. Whereas the aforementioned systems are demonstrated with robust and evident strong coupling effects, they are either non-solid-state or suffering from complex operation conditions, such as ultrahigh vacuum and cryogenic temperature. Theoretically, the coupling strength g, which is equal to half of the RS, is determined by

$$g = \frac{\hbar\omega_{\mathrm{c}}}{\sqrt{2\hbar\varepsilon_0\omega_{\mathrm{d}}V_{\mathrm{eff}}}}\boldsymbol{\mu}_{\mathrm{c}}\cdot\hat{f}_{\mathrm{d}}(\boldsymbol{r}_{\mathrm{c}}),$$

where V_{eff} is the effective mode volume of the cavity, $\boldsymbol{\mu}_{\mathrm{c}}$ and $\boldsymbol{r}_{\mathrm{c}}$ are the dipole moment and location of the emitter, respectively, and $\hat{f}_{\mathrm{d}}(\boldsymbol{r}_{\mathrm{c}})$ is the normalized electric field of the optical cavity.[12] Therefore, to realize strong coupling with large RS, one needs exciton transitions with large transition dipole moment and optical cavities with ultrasmall mode volumes. In addition, excitons with large binding energies are favorable for the room-temperature operation of strong coupling.

In recent years, two-dimensional transition-metal dichalcogenides (TMDs) have attracted significant attention because of their excellent optical and optoelectronic responses associated with their two-dimensional exciton transitions.[13–18] Monolayer TMDs usually exhibit large exci-

*Project supported by the National Natural Science Foundation of China (Grant Nos. 51290271 and 11474364), the National Basic Research Program of China (Grant Nos. 2013CB933601 and 2013YQ12034506), the Natural Science Funds for Distinguished Young Scholars of Guangdong Province, China (Grant No. 2014A030306017), the Pearl River S & T Nova Program of Guangzhou, China (Grant No. 201610010084), and the Guangdong Special Support Program, China.

†Corresponding author. E-mail: chenhj8@mail.sysu.edu.cn

‡Corresponding author. E-mail: stsdsz@mail.sysu.edu.cn

© 2018 Chinese Physical Society and IOP Publishing Ltd

ton binding energies of 0.3–0.9 eV, which is much larger than the thermal activation energy at room temperature (25 meV). In addition, the overlap of the electron–hole wave functions in two-dimensional plane of the monolayer TMDs is very strong because of their atomic thicknesses, which enhances transition dipole moments of the two-dimensional excitons.[19] On the other hand, TMDs can also endow the strong coupling effects with intriguing functionalities that are derived from their specific excitonic characteristics, such as tenability and valley-controlled optical response, which can open up new avenues for both fundamental research and practical applications.[20] Eventually, several studies have demonstrated the strong coupling effects by integrating TMDs with various optical micro- and nanocavities.[21–25]

Recently, we have realized an all-solid-state system exhibiting room-temperature Rabi splitting with active control in a heterostructure consisting of monolayer WS_2 and an individual plasmonic gold nanorod.[26] By taking advantage of the large transition dipole moment of the WS_2 exciton, giant Rabi splitting energies of ~ 133 meV can be achieved at ambient conditions. Practical optoelectronic applications usually require building blocks with multiple functionalities that are derived from different materials. Hence, we generalized the strong coupling studies of TMDs to heterostructures composed of an individual Au nanorod and monolayer WSe_2. In comparison with WS_2, the monolayer WSe_2 exhibits a smaller bandgap and a 10 times higher electron mobility, which has great application potential in infrared optoelectronic devices. We show that the dipolar plasmon resonance of gold nanorod can lead to strong localized electromagnetic fields on the surface of the WSe_2, giving rise to coherent interaction between the two-dimensional excitons and plasmon resonance. Evident anti-crossing behavior can be observed from the coupled energy diagram of the heterostructures, whereby an RS up to 98 meV is extracted. One should note that a recent study has demonstrated the strong coupling effect by integrating the monolayer WSe_2 with an individual silver nanowire, where high-order Fabry-Pérot cavity mode of the nanowire was employed.[27] In our study, the dipolar plasmon resonance mode was utilized, which resulted in a two-times higher RS energy in comparison with the previous study.

2. Experimental methods

2.1. Preparation of gold nanorods–monolayer WSe_2 heterostructures

Gold nanorods were grown using a seed-mediated method.[28] Briefly, the seed solution was prepared by adding a freshly prepared ice-cold $NaBH_4$ aqueous solution (0.6 mL, 0.1 M) into a mixture solution composed of $HAuCl_4$ solution (0.25 mL, 0.01 M) and CTAB solution (9.75 mL, 0.1 M). Afterwards, rapid inversion-mixing was performed for 2 min. The seed solution was kept at room temperature for 2–6 h before use. The growth solution was made by sequential addition of $HAuCl_4$ (2.0 mL, 0.01 M), $AgNO_3$ (0.4 mL, 0.01 M), HCl (0.16 mL, 5 M), and AA (0.32 mL, 0.1 M) to the CTAB solution (40.0 mL, 0.1 M). The gold nanorods were obtained by adding the seed solution (20 μL) into the growth solution. The resulting mixture was left undisturbed at room temperature overnight. The monolayer WSe_2 flake was grown by the chemical vapor deposition (CVD) method. To prepare the heterostructure, the gold nanorods were deposited onto the monolayer WSe_2 flake by drop-casting. Various heterostructures can be obtained after the droplet dried naturally under ambient conditions.

2.2. Spectra measurements

The scattering spectra of individual gold nanorods–WSe_2 heterostructure were recorded on a dark-field optical microscope (Olympus BX51) that was integrated with a quartz-tungsten-halogen lamp (100 W), monochromator (Acton SpectraPro 2360), and charge-coupled device camera (Princeton Instruments Pixis 400BR_eXcelon). The camera was thermoelectrically cooled to -70 °C during the measurements. A dark-field objective (100×, numerical aperture 0.80) was employed for both illuminating the heterostructures with the white excitation light and collecting the scattered light.

The extinction spectra of the gold nanorods aqueous solution were measured on a HITACHIU-4100 UV/visible/near-infrared spectrophotometer. The Raman and photoluminescence (PL) spectra of the monolayer WSe_2 were collected using a Renishaw inVia Reflex system integrated with a dark-field microscope (Leica). The 532-nm excitation laser was focused onto the samples with a diameter of ~ 1 μm through a 50× objective (NA = 0.8).

2.3. Morphology characterizations

SEM images of individual heterostructures were acquired using an FEI Quanta 450 microscope. The thickness of the monolayer WSe_2 was measured using an atomic force microscope (AFM, NTEGRA Spectra). High-resolution transmission electron microscopy (HRTEM) and selected-area electron diffraction measurements were conducted on the same TEM system (FEI Tecnai3 G2 60-300), with an operation voltage of 300 kV.

2.4. Calculations

2.4.1. Finite-difference time-domain (FDTD) calculations

The FDTD method was utilized to calculate the optical properties of the various heterostructures. The individual gold nanorod was modeled as a cylinder capped with hemispheres at each end that was placed on a WSe_2 layer on top of a 300-nm-thick SiO_2 layer. The bulk dielectric function of gold was used for the calculations.[29] The dielectric function of

the monolayer WSe_2 was adopted from previously reported values.[30] In this manner, the exciton energy was determined to be 1.66 eV. A dielectric constant of 2.25 was used for the SiO_2 substrate. For the calculation of scattering spectra of the heterostructures, the lengths and diameters of gold nanorods were set to (78 nm, 26 nm), (80 nm, 25 nm), (81 nm, 24 nm), (83 nm, 24 nm), (86 nm, 24 nm), and (87 nm, 20 nm). The thickness of the WSe_2 monolayer was set to 1 nm.

2.4.2. Coupled harmonic oscillator model

The strong coupling effect can be phenomenologically described using a coupled harmonic oscillator model,[10,25]

$$\begin{pmatrix} E_{\rm pl} + \mathrm{i}\frac{\gamma_{\rm pl}}{2} & g \\ g & E_{\rm ex} + \mathrm{i}\frac{\gamma_{\rm ex}}{2} \end{pmatrix} \begin{pmatrix} \alpha \\ \beta \end{pmatrix} = E_{\pm} \begin{pmatrix} \alpha \\ \beta \end{pmatrix}, \qquad (1)$$

where $E_{\rm pl}$, $E_{\rm ex}$ and $\gamma_{\rm pl}$, $\gamma_{\rm ex}$ are the energies of the uncoupled plasmon and exciton transition and their respective dissipation rates. Parameter g is the coupling strength, $E_{\pm}$ are the eigenvalues of the coupled system, which describe the energies of the hybridized states, and α and β are the coefficients of the linear combination of the plasmon and exciton; $|\alpha|^2 + |\beta|^2 = 1$. To simplify the analysis we ignore the dissipation; thus, the eigenvalues can be obtained as

$$E_{\pm} = \frac{E_{\rm pl} + E_{\rm ex}}{2} \pm \frac{\sqrt{4g^2 + \delta^2}}{2}, \qquad (2)$$

where $\delta = E_{\rm pl} - E_{\rm ex}$ is the detuning between the plasmon resonance and exciton transition energy. The Rabi splitting energy, $\hbar\Omega = 2g$, can be obtained by setting $E_{\rm pl} = E_{\rm ex}$. Therefore, $g = \sqrt{(E_+ - E_{\rm ex})(E_{\rm ex} - E_-)}$.

3. Results and discussion

Usually, the elongated gold nanorods exhibit two types of dipolar plasmon resonances: one is the transverse plasmon mode (TPM) associated with electron oscillations along the diameter direction, and the other is the longitudinal one (LPM) originated from the electron oscillations along the length direction.[31] The operation wavelength of the TPM is usually located at $\sim$ 530 nm irrespective of the aspect ratio of the nanorod. In contrast, the LPMs exhibit wavelengths that are nearly linearly dependent on the aspect ratio of the nanorod.[28] Such a characteristic makes the gold nanorod an excellent nanocavity for studying the strong coupling behavior. By synthetically tuning the nanorod aspect ratio, different LPM wavelengths can be generated allowing us to scan across the fixed exciton transition energy; hence, regimes with varied coupling strengths can be obtained.

By increasing the aspect ratios of the nanorod samples, the LPM wavelengths can be progressively redshifted from 688 nm to 833 nm (Fig. 1). In figure 1(a) the green line shows the extinction spectrum of the pristine aqueous gold nanorod sample, which exhibits an LPM wavelength of 766 nm. The morphologies of the nanorods can be seen clearly from their TEM image, which show uniform size and shape distributions (Fig. 1(b)). The average length, diameter, and aspect ratio of the gold nanorods can thereafter be determined as 80 ± 6 nm, 23 ± 2 nm, and 3.4 ± 0.4, respectively.

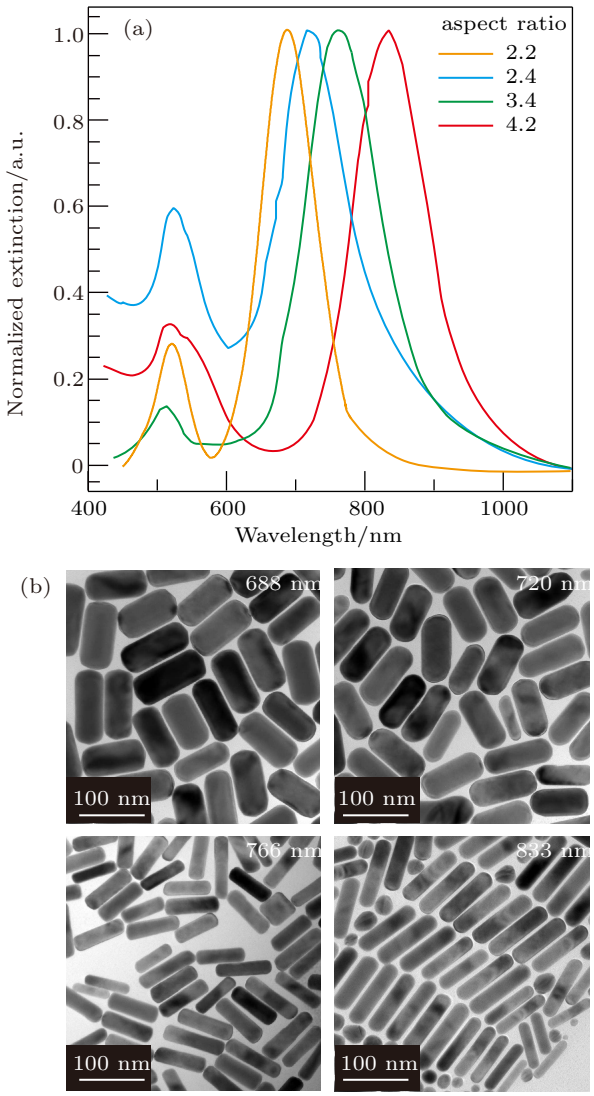


Fig. 1. Gold nanorods with different LPM wavelengths. (a) Extinction spectra of the gold nanorod samples with different aspect ratios. The LPM wavelengths from left to right are 688 nm, 720 nm, 766 nm, and 833 nm, respectively. (b) TEM images of the gold nanorod samples corresponding to panel (a). The aspect ratios of the nanorods increase from left to right.

The WSe_2 sample used in our study had a triangular shape with an edge length of $\sim$ 50 μm (Fig. 2(a)). The monolayer nature of WSe_2 flake was confirmed by its typical AFM image, whereby its thickness was determined to be $\sim$ 0.9 nm (Fig. 2(b)). Figure 2(c) shows the HRTEM image of the WSe_2 flake, which clearly reveals the single-crystalline nature of the sample. Furthermore, the hexagonal crystalline structure of the WSe_2 can be manifested from its SAED pattern (the inset of Fig. 2(c)). The Raman spectrum shown in Fig. 2(d) indicates the absence of the B^1_{2g} mode at $\sim$ 308 cm^{-1}, which is an important signature of the monolayer WSe_2.[32] The excellent uniformity of the sample can be manifested by the Raman intensity mapping across the entire WSe_2 flake (Fig. 2(e)).

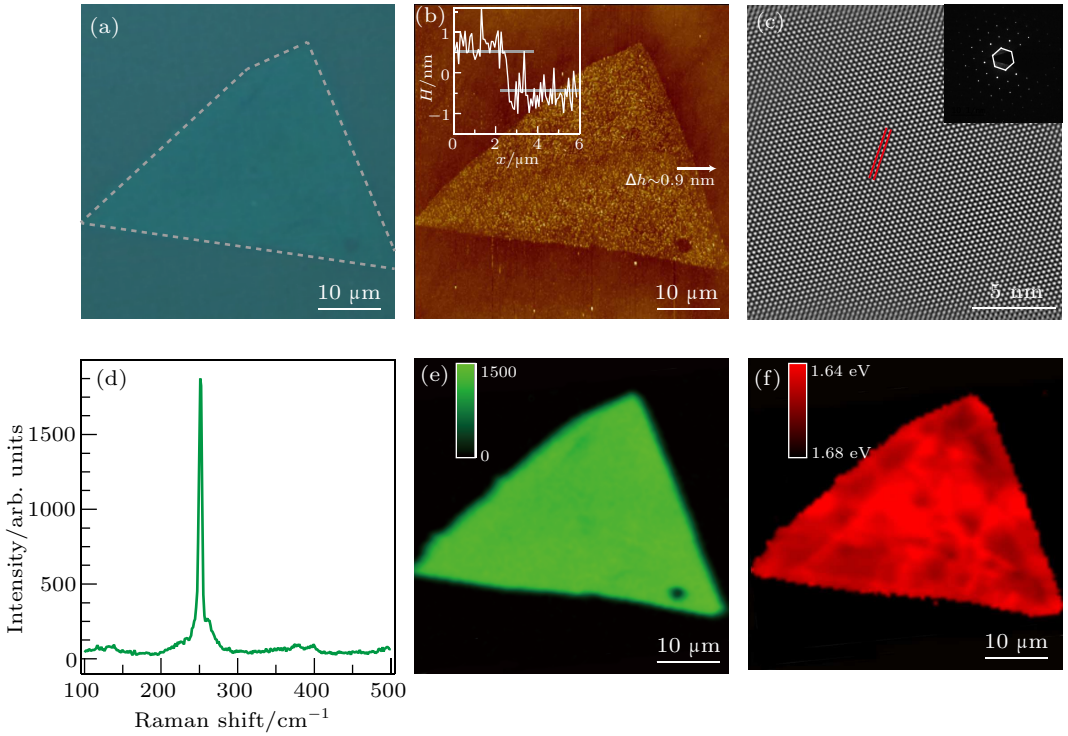


Fig. 2. Characterizations of the monolayer WSe_2 flake. (a) Optical image of the monolayer WSe_2 sample. (b) AFM image of the monolayer WSe_2 flake showing the thickness of ~ 0.9 nm. (c) HRTEM image of the monolayer WSe_2 sample. Inset shows the corresponding SAED pattern, which shows a hexagonal crystalline structure. The red lines indicate the two adjacent crystalline planes. (d) Raman spectrum of the monolayer WSe_2 sample. (e), (f) Raman intensity and PL maximum mapping of the WSe_2 flake corresponding to panel (a), respectively. The Raman mapping is monitored between 200 cm^{-1}–300 cm^{-1}.

In our study, we employed single-particle dark-field scattering microscopy to study the strong coupling effect in an individual heterostructure; it allows us to get rid of extrinsic factors such as the inhomogeneous size distribution of plasmonic nanocrystals, background scattering, or aggregation of nanocrystals.[33,34] To that end, gold nanorods with different aspect ratios were dispersed onto the monolayer WSe_2 flake to form various gold nanorod-WSe_2 heterostructures, whereby a pattern-matching method was employed to correlate the geometry of each heterostructure and its scattering spectrum (Fig. 3(a)).[35] As shown in Fig. 3(b) (upper panel), the pristine monolayer WSe_2 flake exhibits a very sharp and strong exciton emission centering at 1.67 eV with a narrow linewidth ($\hbar\gamma_{ex}$) of 47 meV. Additionally, such an emission characteristic is very uniform across the entire flake (Fig. 2(f)). The pristine gold nanorod with an aspect ratio of 3.5 exhibits a strong light scattering centering at 1.67 eV, which corresponds to its LPM resonance (Fig. 3(b), middle panel). Such LPM energy is in resonance with the exciton transition of the monolayer WSe_2. As a result, when the gold nanorod was placed closely to the WSe_2 surface, its LPM can couple efficiently with the two-dimensional exciton transitions in the WSe_2, giving rise to mode splitting in the scattering spectrum of the individual heterostructure (Fig. 3(b), lower panel). The high-(HEM) and low-energy (LEM) hybrid modes could thereafter be evidently observed (Fig. 1(d), lower panel).

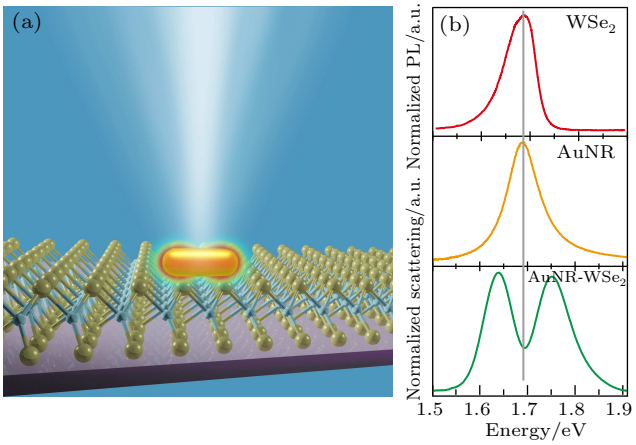


Fig. 3. Gold nanorod-WSe_2 heterostructures. (a) Schematic showing the heterostructure composed of an individual gold nanorod supported by a monolayer WSe_2 flake. (b) Photoluminescence spectrum of the monolayer WSe_2 (upper), scattering spectrum of an individual gold nanorod (middle), and scattering spectrum of an individual gold nanorod-WSe_2 heterostructure (lower).

To thoroughly study the interaction between the LPM and excitons, scattering spectra from various gold nanorod-WSe_2 heterostructures with different detunings between the plasmon and exciton transition energies were measured. The detunings were controlled by selecting heterostructures with specific gold nanorod aspect ratios. Figure 4(a) shows the scattering spectra from seven representative heterostructures. The corresponding nanorod morphologies are illustrated in Fig. 4(b). Upon increase of the nanorod aspect ratios from 3.0

to 4.4, the LPM energies were progressively scanned across the exciton transition energy. Two observations should be noted. First, there always exist two split modes on the scattering spectra of the heterostructures. Second, when the LPM energies are on the high-energy side from the exciton transition, the HEM dominates and redshifts with decreasing LPM energies. As the LPMs become overlapped with the exciton transition, the HEM and LEM are comparable with each other. When the LPM energies move away from the exciton to the low-energy side, the LEM becomes higher than the HEM and redshifts as the detuning energy becomes larger. To further corroborate the experimental spectra, FDTD simulations were conducted to calculate the light scattering properties of the various heterostructures. The shapes and evolvements of the calculated scattering spectra are similar to the experimental ones (Fig. 4(c)). These observations suggest that the interaction between the LPM and excitons is strongly dependent on the overlap between the LPM and exciton transition energies.

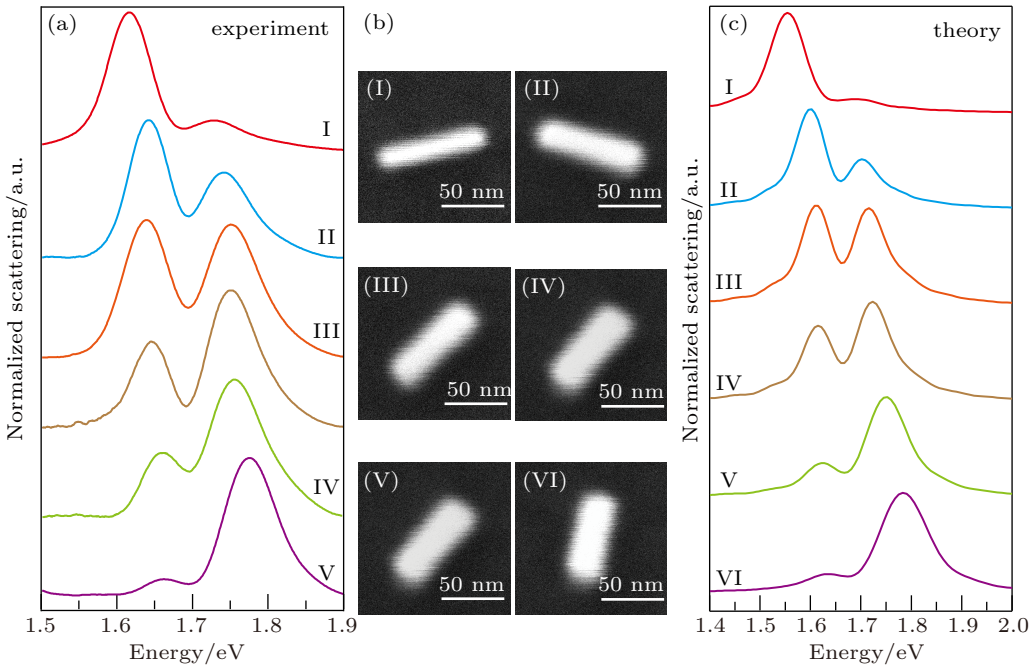


Fig. 4. Light scattering properties of the individual gold nanorod-WSe_2 heterostructures. (a) Dark-field scattering spectra from different individual gold nanorods coupled to the same monolayer WSe_2. (b) SEM images of the gold nanorods with different aspect ratios, which correspond to the scattering spectra shown in panel (a). The aspect ratios of the nanorods from (I) to (VI) are 4.4, 3.6, 3.5, 3.4, 3.2, and 3.0, respectively. (c) Calculated spectra corresponding to the experimental ones shown in panel (a). The intensities of the scattering spectra have been normalized and shifted upward for the purpose of comparison. The grey lines shown in panels (a) and (c) indicate the exciton transition energy.

To further reveal the coupling regime of the heterostructures, the coupled energy diagram demonstrating the dependence of the two hybrid modes on the detunings was inspected. As shown in Fig. 5(a), two distinct branches associated with the LEM (lower branch) and HEM (higher branch) can be clearly seen in the coupled energy diagram. Moreover, these two branches demonstrate clear anti-crossing behavior, suggesting a coherent interaction between the exciton and LPM resonance of the nanorod. We then utilized a coupled harmonic oscillator model to describe the anti-crossing behavior,[10] which shows excellent agreement with the experimental results. Thus, the RS energy, $\hbar\Omega$, can be found to be 98 meV at zero energy detuning. The criterion that separates a strong coupling regime from weak coupling is given by[21]

$$\hbar\Omega > \frac{\hbar\gamma_{\rm pl} + \hbar\gamma_{\rm ex}}{2},$$

where $\gamma_{\rm pl}$ is the linewidth of the LPM resonance. In our study, $\hbar\gamma_{\rm pl}$ and $\hbar\gamma_{\rm ex}$ are 82 meV and 47 meV, respectively. As a result, an RS energy of 98 meV suggests that the interaction between the LPM resonance and exciton transition in an individual heterostructure at zero detuning satisfies the condition for the strong coupling regime. In this regime, hybridized states with part-light and part-matter characteristics are formed because of the coherent energy exchange between the exciton and LPM resonance. The coupled harmonic oscillator model was then utilized to further calculate the respective contributions from the exciton and plasmon components for the upper and lower branches. As shown in Fig. 5(b), by detuning the plasmon resonance to the low-energy side of the exciton transition, the lower branch is more plasmon-like while the high-energy one is more exciton-like, and vice versa for detuning to the high-energy side.

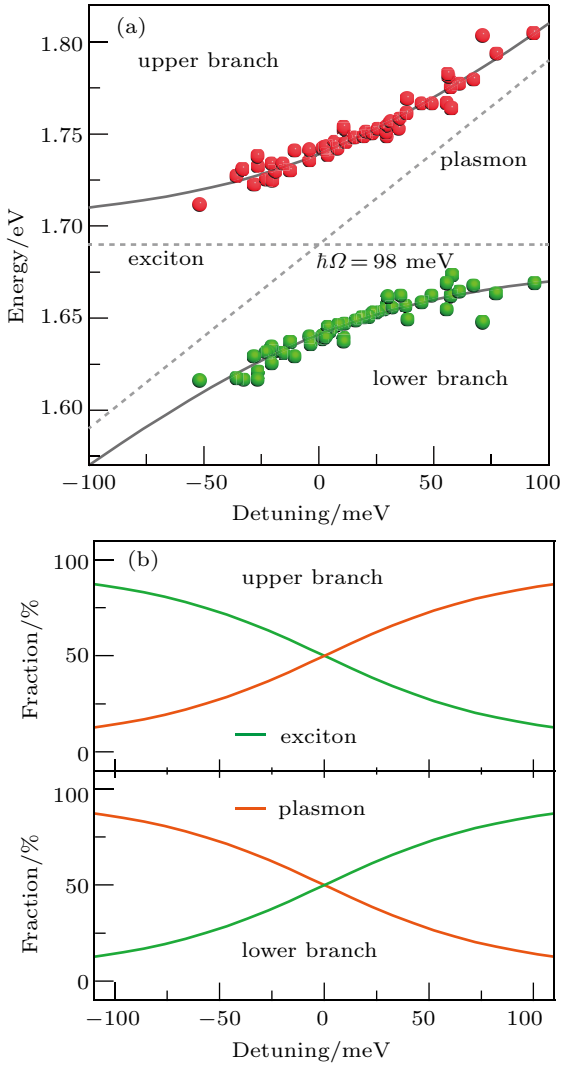


Fig. 5. Strong coupling of the gold nanorod-WSe_2 heterostructures. (a) Resonance peaks as a function of the detuning energies between the LPM resonance and exciton transition. The red and green dots are extracted peaks from experimental measurements. The black solid lines are fitting results according to the coupled harmonic oscillator model, which demonstrate the anticrossing behavior. The horizontal dashed line indicates the exciton transition energy, while the diagonal one stands for the dispersion of the LPM resonances. (b) Exciton and plasmon fractions of the upper and lower branches of the heterostructures.

The strong coupling between the LPM resonance and exciton transition is mediated by the localized plasmonic field.[12,36] Namely, the nanorod acts as an antenna to focus the free-space electromagnetic field into the gap between the nanorod and WSe_2. Such a localized field can thereafter excite the exciton transition of the WSe_2. As a result, energy transfer between the plasmonic field and transition dipole moment can occur when the exciton is in its excited state. According to this coupling mechanism, the strong coupling should be rigorously dependent on the separation between the nanorod and WSe_2. Figure 6 shows the calculated scattering spectra from heterostructures with different gaps between the gold nanorod and the WSe_2 surface. As the gold nanorod is kept away from the WSe_2, the split modes vanish quickly and disappear for separations larger than 1.5 nm. Such a behavior suggests that the coupling is mediated by the plasmonic near-field located within the gap between the nanorod and WSe_2.

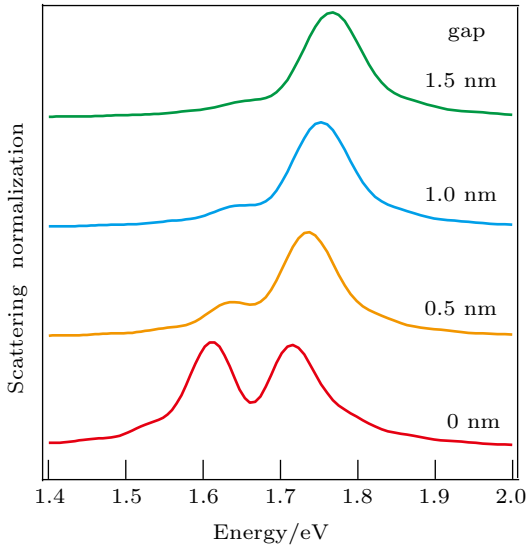


Fig. 6. Calculated scattering spectra of heterostructures with different separations between the gold nanorod and the WSe_2 surface. The aspect ratio of the gold nanorod is kept as 3.5.

The all-solid-state strong coupling system revealed in our study might have great potential in future quantum information technology, where long coherence time of the qubits is desired. However, in our current study the experimental configuration is very simple and only suitable for revealing the underlying beautiful physics. To make practical devices that are compatible with transmitting and processing information nowadays, one needs to expand the individual Au nanorod-WSe_2 heterostructure into an array structure. In such a manner, the array structure can be excited by a laser beam that is focused down to the diffraction-limit scale as used in many nanophotonic devices. In addition, the optical response of the array can be collected and characterized by ordinary reflection and transmission microscopy, which are more compatible with optical systems nowadays.

4. Conclusion

In summary, we have revealed the strong coupling effect between the LPM resonance of an individual gold nanorod and two-dimensional exciton in monolayer WSe_2 flake. By employing single-particle dark-field scattering spectroscopy, strong coupling with evident RS was observed from the scattering spectra of the gold nanorod-WSe_2 heterostructures. In addition, anti-crossing behavior was revealed from the coupled energy diagram by changing the energy detunings between the LPM resonance and exciton transition, where an RS energy of 98 meV was extracted. We believe that the proposed gold nanorod-WSe_2 heterostructures can pave the way for exploring the strong coupling of all-solid-state systems in the near-infrared regime, which has a potential for application in future

quantum optics and quantum information processing technologies.

References

[1] Koenderink A F, Alù A and Polman A 2015 *Science* **348** 516
[2] Yoshie T, Scherer A, Hendrickson J, Khitrova G, Gibbs H M, Rupper G, Ell C, Shchekin O B and Deppe D G 2004 *Nature* **432** 200
[3] Matsukevich D N and Kuzmich A 2004 *Science* **306** 663
[4] Chen W, Beck K M, Bücker R, Gullans M, Lukin M D, Tanji-Suzuki H and Vuletić V 2013 *Science* **341** 768
[5] Sanvitto D and Kéna-Cohen S 2016 *Nat. Mater.* **15** 1061
[6] Hood C J, Lynn T W, Doherty A C, Parkins A S and Kimble H J 2000 *Science* **287** 1447
[7] Reithmaier J R, Sęk G, Löffler A, Hofmann C, Kuhn S, Reitzenstein S, Keldysh L V, Kulakovskii V D, Reinecke T L and Forchel A 2004 *Nature* **432** 197
[8] Savona V, Andreani L C, Schwendimann P and Quattropani A 1995 *Solid State Commun.* **93** 733
[9] Fofang N T, Park T H, Neumann O, Mirin N A, Nordlander P and Halas N J 2008 *Nano Lett.* **8** 3481
[10] Zengin G, Wersäll M, Nilsson S, Antosiewicz T J, Käll M and Shegai T 2015 *Phys. Rev. Lett.* **114** 157401
[11] Santhosh K, Bitton O, Chuntonov L and Haran G 2016 *Nat. Commun.* **7** 11823
[12] Liu R M, Zhou Z K, Yu Y C, Zhang T W, Wang H, Liu G H, Wei Y M, Chen H J and Wang X H 2017 *Phys. Rev. Lett.* **118** 237401
[13] Zhang H 2015 *ACS Nano* **9** 9451
[14] Zhou K G and Zhang H L 2015 *Small* **11** 3206
[15] Mak K F and Shan J 2016 *Nat. Photon.* **10** 216
[16] Liu M, Zheng X U, Qi Y L, Liu H, Luo A Y, Luo Z C, Xu W C, Zhao C J and Zhang H 2014 *Opt. Express* **22** 22841
[17] Luo Z Q, Wu D D, Xu B, Xu H Y, Cai Z P, Peng J, Weng J, Xu S, Zhu C H, Wang F Q, Sun Z P and Zhang H 2016 *Nanoscale* **8** 1066
[18] Jiang Y Q, Miao L L, Jiang G B, Chen Y, Qi X, Jiang X F, Zhang H and Wen S C 2015 *Sci. Rep.* **5** 16372
[19] Ye Z L, Cao T, Brien K O, Zhu H Y, Yin X B, Wang Y, Louie S G and Zhang X 2014 *Nature* **513** 214
[20] Schaibley J R, Yu H Y, Clark G, Rivera P, Ross J S, Seyler K L, Yao W and Xu X D 2016 *Nat. Rev. Mats.* **1** 16055
[21] Dufferwiel S, Schwarz S, Withers F, Trichet A A P, Li F, Sich M, Del Pozo-Zamudio O, Clark C, Nalitov A, Solnyshkov D D, Malpuech G, Novoselov K S, Smith J M, Skolnick M S, Krizhanovskii D N and Tartakovskii A I 2015 *Nat. Commun.* **6** 8579
[22] Liu X Z, Galfsky T, Sun Z, Xia F N, Lin E C, Lee Y H, Kéna-Cohen S and Menon V M 2015 *Nat. Photon.* **9** 30
[23] Lundt N, Klembt S, Cherotchenko E, Betzold S, Iff O, Nalitov A V, Klaas M, Dietrich C P, Kavokin A V, Höfling S and Schneider C 2016 *Nat. Commun.* **7** 13328
[24] Liu W J, Lee B, Naylor C H, Ee H S, Park J, Johnson A T and Agarwal R 2016 *Nano Lett.* **16** 1262
[25] Wang S J, Li S L, Chervy T, Shalabney A, Azzini S, Orgiu E, Hutchison J A, Genet C, Samorì P and Ebbesen T W 2016 *Nano Lett.* **16** 4368
[26] Wen J X, Wang H, Wang W L, Deng Z X, Zhuang C, Zhang Y, Liu F, She J C, Chen J, Chen H J, Deng S Z and Xu N S 2017 *Nano Lett.* **17** 4689
[27] Zheng D, Zhang S P, Deng Q, Kang M, Nordlander P and Xu H X 2017 *Nano Lett.* **17** 3809
[28] Gole A and Murphy C J 2004 *Chem. Mater.* **16** 3633
[29] Johnson P B and Christy R W 1972 *Phys. Rev. B* **6** 4370
[30] Li Y, Chernikov A, Zhang X, Rigosi A, Hill H M, van der Zande A M, Chenet D A, Shih E M, Hone J and Heinz T F 2014 *Phys. Rev. B* **90** 205422
[31] Huang X H, Neretina S and El-Sayed M A 2009 *Adv. Mater.* **21** 4880
[32] Zhao W, Ghorannevis Z, Amara K K, Pang J R, Toh M, Zhang X, Kloc C, Tan P H and Eda G 2013 *Nanoscale* **5** 9677
[33] Chen H J, Shao L, Ming T, Woo K C, Man Y C, Wang J F and Lin H Q 2011 *ACS Nano* **5** 6754
[34] Chen H J, Sun Z H, Ni W H, Woo K C, Lin H Q, Sun L D, Yan C H and Wang J F 2009 *Small* **5** 2111
[35] Ming T, Zhao L, Xiao M D and Wang J F 2010 *Small* **6** 2514
[36] Wang H, Ke Y L, Xu N S, Zhan R Z, Zheng Z B, Wen J X, Yan J H, Liu P, Chen J, She J C, Zhang Y, Liu F, Chen H J and Deng S Z 2016 *Nano Lett.* **16** 6886